Scale-Dependent Models for Atmospheric Flows

Rupert Klein

FB Mathematik und Informatik, Freie Universität Berlin, 14195 Berlin, Germany; email: rupert.klein@math.fu-berlin.de

Annu. Rev. Fluid Mech. 2010. 42:249–74

First published online as a Review in Advance on August 25, 2009

The *Annual Review of Fluid Mechanics* is online at fluid.annualreviews.org

This article's doi: 10.1146/annurev-fluid-121108-145537

0066-4189/10/0115-0249$20.00

Key Words

meteorology, multiple scales

Abstract

Atmospheric flows feature length scales from 10^{-5} to 10^{5} m and timescales from microseconds to weeks or more. For scales above several kilometers and minutes, there is a natural scale separation induced by the atmosphere's thermal stratification, together with the influences of gravity and Earth's rotation, and the fact that atmospheric-flow Mach numbers are typically small. A central aim of theoretical meteorology is to understand the associated scale-specific flow phenomena, such as internal gravity waves, baroclinic instabilities, Rossby waves, cloud formation and moist convection, (anti-)cyclonic weather patterns, hurricanes, and a variety of interacting waves in the tropics. Single-scale asymptotics yields reduced sets of equations that capture the essence of these scale-specific processes. For studies of interactions across scales, techniques of multiple-scales asymptotics have received increasing recognition in recent years. This article recounts the most prominent scales and associated scale-dependent models and summarizes recent multiple-scales developments.

1. INTRODUCTION

1.1. Characteristic Scales and Dimensionless Parameters

Potential temperature (Θ): temperature an air parcel would attain if compressed adiabatically to the sea-level pressure

Barotropic versus baroclinic: barotropic distributions of a variable have a unique sign over the depth of the fluid column, whereas baroclinic ones do not

Internal waves: oscillations with gravity as the restoring force

Thermal wind: vertical shear induced by horizontal potential-temperature gradients under hydrostatic and geostrophic balance (see Section 2.2.2)

Here we borrow from Keller & Ting (1951) and Klein (2000, 2004, 2008) to argue for an inherent scale separation in large-scale atmospheric flows. **Table 1** lists eight universal characteristics of atmospheric motions involving the physical dimensions of length, time, mass, and temperature. Earth's radius, its rotation rate, and the acceleration of gravity are obviously universal. The sea-level pressure is set by the mass (weight) of the atmosphere, which is essentially constant in time. The water-freezing temperature is a good reference value for the large-scale, long-time-averaged conditions on Earth (see also Rahmstorf et al. 2004 for the related paleoclimatic record). The equator-to-pole potential-temperature difference is maintained by the inhomogeneous irradiation from the Sun, and its magnitude appears to be stable over very long periods of time. An average vertical potential-temperature difference across the troposphere is of the same order of magnitude as the equator-to-pole temperature difference (see Frierson 2008, Schneider 2006, and references therein). Finally the dry-air gas constant is a good approximation to local values because the mass fractions of water vapor and greenhouse gases are very small. These seven dimensional characteristics allow for three independent, dimensionless combinations in addition to the isentropic exponent γ. A possible choice is

$$\begin{aligned} \Pi_1 &= \frac{h_{sc}}{a} \sim 1.6 \times 10^{-3}, \\ \Pi_2 &= \frac{\Delta\Theta}{T_{ref}} \sim 1.5 \times 10^{-1}, \\ \Pi_3 &= \frac{c_{ref}}{\Omega a} \sim 4.7 \times 10^{-1}, \end{aligned} \tag{1}$$

where h_{sc} is the density scale height, and c_{ref} is of the order of a characteristic speed of sound or of barotropic (external) gravity waves, as given in the first three items of **Table 2**. The last two items in **Table 2** are further characteristic signal speeds derived from the quantities of **Table 1**: c_{int} corresponds to the horizontal phase speed of linearized internal gravity waves in the long-wavelength limit (see Gill 1982, chapter 6). In estimating a typical horizontal flow velocity, we use the thermal wind relation (see Equation 15 below) applied to planetary scales, and let $u_{ref} \sim h_{sc}|\partial u/\partial z|_{thermal}$ and $\nabla_\parallel \bar{\theta} \sim \Delta\Theta/\frac{\pi}{2}a$, with $\nabla_\parallel$ as the horizontal gradient. Importantly, internal gravity waves are dispersive, and their phase speed depends strongly on the wave-number vector, so that c_{int} is merely an upper estimate. Internal wave signals may move at speeds comparable to u_{ref} in practice (see also Sections 2.3 and 4.3 below).

Let us consider now the distances that sound waves, internal waves, and particles advected by the thermal wind would travel during the characteristic time of Earth's rotation, $1/\Omega \sim 10^4$ s.

Table 1 Universal characteristics of atmospheric motions

Earth's radius	$a \sim 6 \times 10^6$ m
Earth's rotation rate	$\Omega \sim 10^{-4}$ s^{-1}
Acceleration of gravity	$g \sim 9.81$ ms^{-2}
Sea-level pressure	$p_{ref} \sim 10^5$ kgm^{-1} s^{-2}
H_2O freezing temperature	$T_{ref} \sim 273$ K
Equator-pole potential temperature difference Tropospheric vertical potential temperature difference	$\Delta\Theta \sim 40$ K
Dry gas constant	$R = 287$ m^2 s^{-2} K^{-1}
Dry isentropic exponent	$\gamma = 1.4$

Table 2 Auxiliary quantities of interest derived from those in Table 1

Sea-level air density	$\rho_{\mathrm{ref}} = p_{\mathrm{ref}}/(RT_{\mathrm{ref}}) \sim 1.25\ \mathrm{kgm}^{-3}$
Density scale height	$h_{\mathrm{sc}} = \gamma p_{\mathrm{ref}}/(g\rho_{\mathrm{ref}}) \sim 11\ \mathrm{km}$
Sound speed	$c_{\mathrm{ref}} = \sqrt{\gamma p_{\mathrm{ref}}/\rho_{\mathrm{ref}}} \sim 330\ \mathrm{ms}^{-1}$
Internal wave speed	$c_{\mathrm{int}} = \sqrt{g h_{\mathrm{sc}} \frac{\Delta\Theta}{T_{\mathrm{ref}}}} \sim 110\ \mathrm{ms}^{-1}$
Thermal wind velocity	$u_{\mathrm{ref}} = \frac{2}{\pi} \frac{g h_{\mathrm{sc}}}{\Omega a} \frac{\Delta\Theta}{T_{\mathrm{ref}}} \sim 12\ \mathrm{ms}^{-1}$

Together with the density scale height, h_{sc}, and the equator-to-pole distance, L_{p}, we find the hierarchy of characteristic lengths displayed in **Table 3**. The technical terms in the left column are often used for these scales in the meteorological literature. The synoptic reference scale, L_{Ro}, is also called the Rossby radius, and the Obukhov scale is frequently termed the external Rossby radius. These length scales are naturally induced by fluid dynamical processes in the atmosphere, and they give rise to multiple-scales regimes when the characteristic signal speeds differ significantly. If we fix, in turn, a length scale to be considered, then the different characteristic signal speeds give rise to multiple times instead of multiple lengths. In general situations, one is faced with combined multiple length–multiple time regimes.

1.2. Distinguished Limits

Even for the simple problem of the linear oscillator with small mass and small damping, an asymptotic expansion that allows for independent variation of the two parameters is bound to fail because limits taken in the space of the mass and damping parameters turn out to be path dependent (Klein 2008). If that is so even for a simple linear problem, there is little hope for independent multiple-parameter expansions in more complex fluid dynamical problems. Therefore, faced with multiple small parameters as in **Table 1**, we proceed by introducing distinguished limits, or coupled limit processes: The parameters are functionally related, and asymptotic analyses proceed in terms of a single expansion parameter only.

The characteristic signal speeds from **Table 2** are compatible with the scalings

$$\frac{c_{\mathrm{int}}}{c_{\mathrm{ref}}} \sim 1/3 \sim \sqrt{\varepsilon}, \quad \frac{u_{\mathrm{ref}}}{c_{\mathrm{int}}} \sim 1/9 \sim \varepsilon, \quad \text{and} \quad \frac{u_{\mathrm{ref}}}{c_{\mathrm{ref}}} \sim \varepsilon^{\frac{3}{2}}, \tag{2}$$

and this corresponds to letting

$$\Pi_1 = c_1\varepsilon^3, \quad \Pi_2 = c_2\varepsilon, \quad \Pi_3 = c_3\sqrt{\varepsilon}, \tag{3}$$

with $c_i = O(1)$ as $\varepsilon \to 0$ for the parameters in **Table 1**. The length scales in **Table 3** then obey

$$L_{\mathrm{meso}} = \frac{h_{\mathrm{sc}}}{\varepsilon}, \quad L_{\mathrm{Ro}} = \frac{h_{\mathrm{sc}}}{\varepsilon^2}, \quad L_{\mathrm{Ob}} = \frac{h_{\mathrm{sc}}}{\varepsilon^{\frac{5}{2}}}, \quad L_p = \frac{h_{\mathrm{sc}}}{\varepsilon^3}. \tag{4}$$

Table 3 Hierarchy of physically distinguished scales in the atmosphere

Planetary scale	$L_{\mathrm{p}} = \frac{\pi}{2}a \sim 10000\ \mathrm{km}$
Obukhov radius	$L_{\mathrm{Ob}} = \frac{c_{\mathrm{ref}}}{\Omega} \sim 3300\ \mathrm{km}$
Synoptic scale	$L_{\mathrm{Ro}} = \frac{c_{\mathrm{int}}}{\Omega} \sim 1100\ \mathrm{km}$
Meso-β scale	$L_{\mathrm{meso}} = \frac{u_{\mathrm{ref}}}{\Omega} \sim 150\ \mathrm{km}$
Meso-γ scale	$h_{\mathrm{sc}} = \frac{\gamma p_{\mathrm{ref}}}{g\rho_{\mathrm{ref}}} \sim 11\ \mathrm{km}$

THE ARGUMENT FOR DISTINGUISHED ASYMPTOTIC LIMITS

The asymptotic behavior of multiple-parameter, singularly perturbed systems is generally path dependent; i.e., their behavior for vanishing singular perturbation parameters depends on the path along which the tuple of parameters approaches its limiting value. Let us consider for illustration the governing equation of a linear oscillator with small mass and small damping, i.e.,

$$\varepsilon\ddot{y} + \delta\dot{y} + y = f(t), \quad \varepsilon, \delta \ll 1.$$

There is a critical level of damping, with $\delta_{\text{crit}} = \kappa\sqrt{\varepsilon}$, that demarcates a regime transition in the behavior of the system for some suitable value of the coefficient κ. For $\delta \geq \delta_{\text{crit}}$, the unforced eigenmodes of the oscillator monotonously decay to $y = 0$, and the displacement y never changes sign. For $\delta < \delta_{\text{crit}}$, one instead observes damped, oscillatory motions. The two extremes of sequential limits exhibit the key point most clearly: If we first let the mass ε vanish and then choose some small δ, we will find a purely damped, nonoscillatory motion with y dropping to zero exponentially on a timescale $t \sim \delta$. In contrast, if we first let $\delta \to 0$, and then choose some $\varepsilon \ll 1$, we find rapid undamped oscillations with characteristic frequency of order $O(\sqrt{\varepsilon})$. These two limiting behaviors are incompatible with each other, even though both arise as $\varepsilon, \delta \to 0$.

Distinguished limits of the form $\delta = d(\varepsilon)$ as $\varepsilon \to 0$ allow us to explicitly specify such limiting paths in the space of parameters and to access different asymptotic regimes in a controlled fashion.

1.3. Governing Equations

To simplify notations, we use the tangent plane approximation throughout this review.

1.3.1. Classical formulation. The compressible flow equations for an ideal gas with constant specific-heat capacities and including gravity, rotation, and generalized source terms serve as the basis for the subsequent discussions. We nondimensionalize using $\ell_{\text{ref}} = h_{\text{sc}}$ and $t_{\text{ref}} = h_{\text{sc}}/u_{\text{ref}}$ for space and time, and p_{ref}, T_{ref}, R, and u_{ref} from **Tables 1** and **2** for the thermodynamic variables and velocity. In addition, we employ the distinguished limits from Equations 2 and 3. The governing equations for the dimensionless horizontal and vertical flow velocities $\boldsymbol{v}_{||}$ and w, pressure p, density ρ, and potential temperature $\Theta = p^{1/\gamma}/\rho$, as functions of the horizontal and vertical coordinates $\boldsymbol{x}$ and z, and time t, then read

$$\left(\frac{\partial}{\partial t} + \boldsymbol{v}_{||}\cdot\nabla_{||} + w\frac{\partial}{\partial z}\right)\boldsymbol{v}_{||} + \varepsilon(2\boldsymbol{\Omega}\times\boldsymbol{v})_{||} + \frac{1}{\varepsilon^3\rho}\nabla_{||}p = \boldsymbol{Q}_{\boldsymbol{v}_{||}}, \tag{5a}$$

$$\left(\frac{\partial}{\partial t} + \boldsymbol{v}_{||}\cdot\nabla_{||} + w\frac{\partial}{\partial z}\right)w + \varepsilon(2\boldsymbol{\Omega}\times\boldsymbol{v})_{\perp} + \frac{1}{\varepsilon^3\rho}\frac{\partial p}{\partial z} = Q_w - \frac{1}{\varepsilon^3}, \tag{5b}$$

$$\left(\frac{\partial}{\partial t} + \boldsymbol{v}_{||}\cdot\nabla_{||} + w\frac{\partial}{\partial z}\right)\rho + \rho\nabla\cdot\boldsymbol{v} = 0, \tag{5c}$$

$$\left(\frac{\partial}{\partial t} + \boldsymbol{v}_{||}\cdot\nabla_{||} + w\frac{\partial}{\partial z}\right)\Theta = Q_\Theta. \tag{5d}$$

Here $\boldsymbol{b}_{||}$ denotes the horizontal component of a vector $\boldsymbol{b}$. The terms $Q_{[\cdot]}$ stand for general source terms, molecular transport, and further unresolved-scale closure terms.

Tangent plane approximation: for horizontal scales much smaller than Earth's circumference, one neglects its sphericity, although not the variation of the Coriolis parameter

1.3.2. Some revealing transformations. Here we introduce a general transformation of both the dependent and independent variables that allows us to reveal the space, time, and amplitude scalings associated with a range of classical atmospheric flow regimes in a unified fashion. For example, we

find that the rescaled horizontal coordinate $\boldsymbol{\xi} = \varepsilon^2 \boldsymbol{x}$ resolves the synoptic spatial scale, that $\tau = \varepsilon^2 t$ resolves the corresponding advection timescale, and that typical relative variations of the pressure and potential temperature associated with synoptic scale motions in quasi-geostrophic balance are $O(\varepsilon^2)$. Once we insert these scalings into the governing equations, it becomes a straightforward matter to identify the dominant balances and to extract the related leading-order approximate equations. In most cases, these leading-order equations already constitute the reduced flow model relevant to the flow regime under consideration.

Exner pressure function: convenient variable in the context of atmosphere flow modeling $\pi = (p/p_{\mathrm{ref}})^{(\gamma-1)/\gamma}$

Hydrostatic balance: pressure gradient balancing the weight of the fluid

The Exner pressure. For the analysis of atmospheric flows, the Exner pressure $\pi = p^{\Gamma}$ with $\Gamma = (\gamma - 1)/\gamma$ turns out to be a convenient variable. The pressure is always in hydrostatic balance to leading order in the atmosphere. For a given horizontally averaged mean stratification of the potential temperature, $\bar{\Theta}(z)$, the corresponding hydrostatic pressure will satisfy $d\bar{p}/dz = -\overline{\rho} = -\bar{p}^{1/\gamma}/\bar{\Theta}$ [see the $O(1/\varepsilon^3)$ terms in Equation 5b]. The exact solution with $\bar{p}(0) = 1$ is

$$\bar{p}(z) = \bar{\pi}(z)^{\frac{1}{\Gamma}}, \quad \text{where} \quad \bar{\pi}(z) = 1 - \Gamma \int_0^z \frac{1}{\bar{\Theta}(z')} dz'. \tag{6}$$

Thus the Exner pressure captures the essential vertical variation of the hydrostatic background pressure due to the atmosphere's stratification without exhibiting the strong drop of the pressure $\bar{p}$ due to the compressibility of air. For example, for a neutrally stratified atmosphere with $\bar{\Theta} \equiv \text{const}$, $\bar{\pi}$ is linear in z, whereas $\bar{p}$ is a strongly nonlinear function. Most atmospheric-flow phenomena may be understood as perturbations away from such a hydrostatically balanced background state.

A general scale transformation. Suppose we are interested in solutions to Equation 5 with a characteristic time $T = t_{\mathrm{ref}}/\varepsilon^{\alpha_t}$ and a horizontal characteristic length $L = h_{\mathrm{sc}}/\varepsilon^{\alpha_x}$ with $\alpha_t, \alpha_x > 0$. Appropriate rescaled coordinates would be

$$\tau = \varepsilon^{\alpha_t} t \quad \text{and} \quad \boldsymbol{\xi} = \varepsilon^{\alpha_x} \boldsymbol{x}. \tag{7}$$

Furthermore, we take into account that the relative (vertical) variation of the potential temperature in the atmosphere is of order $O(\Delta\Theta/T_{\mathrm{ref}}) = O(\varepsilon)$ and that the vertical and horizontal velocities in most regimes to be considered scale as $|w|/|\boldsymbol{v}_{\|}| \sim h_{\mathrm{sc}}/L = O(\varepsilon^{\alpha_x})$. This suggests new dependent variables,

$$\begin{aligned} \Theta(\tau, \boldsymbol{\xi}, z) &= 1 + \varepsilon\bar{\theta}(z) + \varepsilon^{\alpha_\pi}\tilde{\theta}(\tau, \boldsymbol{\xi}, z), \\ \pi(\tau, \boldsymbol{\xi}, z) &= \bar{\pi}(z) + \varepsilon^{\alpha_\pi}\Gamma\tilde{\pi}(\tau, \boldsymbol{\xi}, z), \\ w(\tau, \boldsymbol{\xi}, z) &= \varepsilon^{\alpha_x}\tilde{w}(\tau, \boldsymbol{\xi}, z), \end{aligned} \tag{8}$$

with $\bar{\pi}(z)$ from Equation 6 for $\bar{\Theta}(z) = 1 + \varepsilon\bar{\theta}(z)$. Then the governing equations become

$$\left(\frac{\varepsilon^{\alpha_t}}{\varepsilon^{\alpha_x}}\frac{\partial}{\partial\tau} + \boldsymbol{v}_{\|}\cdot\nabla_{\boldsymbol{\xi}} + \tilde{w}\frac{\partial}{\partial z}\right)\boldsymbol{v}_{\|} + \frac{(2\boldsymbol{\Omega}\times\boldsymbol{v})_{\|}}{\varepsilon^{\alpha_x-1}} + \frac{\varepsilon^{\alpha_\pi}}{\varepsilon^3}\Theta\nabla_{\boldsymbol{\xi}}\tilde{\pi} = \boldsymbol{Q}^{\varepsilon}_{\boldsymbol{v}_{\|}}, \tag{9a}$$

$$\left(\frac{\varepsilon^{\alpha_t}}{\varepsilon^{\alpha_x}}\frac{\partial}{\partial\tau} + \boldsymbol{v}_{\|}\cdot\nabla_{\boldsymbol{\xi}} + \tilde{w}\frac{\partial}{\partial z}\right)\tilde{w} + \frac{(2\boldsymbol{\Omega}\times\boldsymbol{v})_{\perp}}{\varepsilon^{2\alpha_x-1}} + \frac{\varepsilon^{\alpha_\pi}}{\varepsilon^{3+2\alpha_x}}\left(\Theta\frac{\partial\tilde{\pi}}{\partial z} - \frac{\tilde{\theta}}{\Theta}\right) = Q^{\varepsilon}_{w}, \tag{9b}$$

$$\left(\frac{\varepsilon^{\alpha_t}}{\varepsilon^{\alpha_x}}\frac{\partial}{\partial\tau} + \boldsymbol{v}_{\|}\cdot\nabla_{\boldsymbol{\xi}} + \tilde{w}\frac{\partial}{\partial z}\right)\tilde{\pi} + \frac{\gamma\pi}{\varepsilon^{\alpha_\pi}}\left(\nabla_{\boldsymbol{\xi}}\cdot\boldsymbol{v}_{\|} + \frac{\partial\tilde{w}}{\partial z} + \frac{\tilde{w}}{\gamma\Gamma\pi}\frac{d\bar{\pi}}{dz}\right) = \frac{\gamma\pi Q^{\varepsilon}_{\Theta}}{\Theta}, \tag{9c}$$

$$\left(\frac{\varepsilon^{\alpha_t}}{\varepsilon^{\alpha_x}}\frac{\partial}{\partial\tau} + \boldsymbol{v}_{\|}\cdot\nabla_{\boldsymbol{\xi}} + \tilde{w}\frac{\partial}{\partial z}\right)\tilde{\theta} + \frac{\varepsilon}{\varepsilon^{\alpha_\pi}}\tilde{w}\frac{d\bar{\theta}}{dz} = Q^{\varepsilon}_{\Theta}. \tag{9d}$$

Below we assume that the source terms, $Q^{\varepsilon}_{[\cdot]}$, are of sufficiently high order in ε to not affect the leading-order asymptotics.

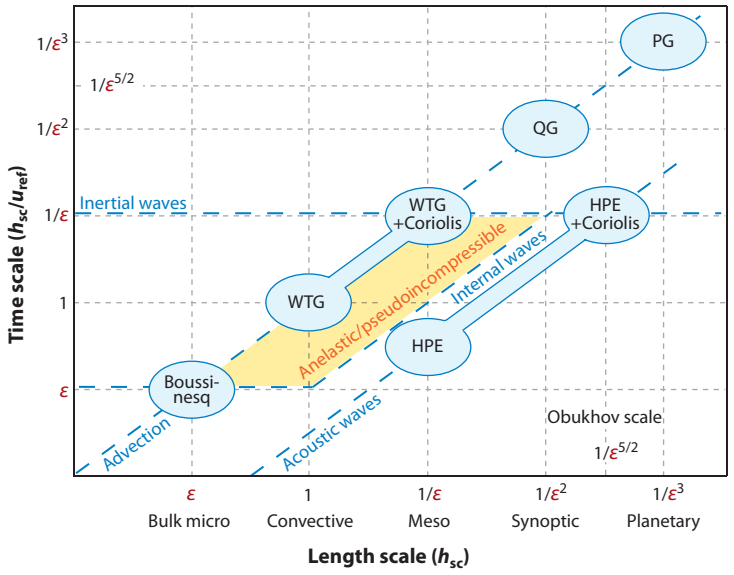

Figure 1

Scaling regimes and model equations for atmospheric flows. The weak-temperature-gradient (WTG) and hydrostatic primitive equation (HPE) models cover a wide range of spatial scales assuming the associated advective and acoustic timescales, respectively. The anelastic and pseudoincompressible models for realistic flow regimes cover multiple spatiotemporal scales (Section 4.3). For similar graphs for near-equatorial flows, see Majda 2007b, Majda & Klein 2003. PG, planetary geostrophic; QG, quasi-geostrophic.

Importantly, in writing Equation 9, we have merely adopted a transformation of variables, but no approximations. Together with the definitions in Equations 7 and 8, they are equivalent to the original version of the compressible flow equations in Equation 5. However, below we employ judicious choices for the scaling exponents, $\alpha_{[\cdot]}$, and assume solutions that adhere to the implied scalings in that $\boldsymbol{v}_{||}, \tilde{w}, \tilde{\pi}, \tilde{\theta} = O(1)$ and that the partial derivative operators ∂_τ, $\nabla_{\boldsymbol{\xi}}$, and ∂_z yield $O(1)$ results when applied to these variables as $\varepsilon \to 0$. This allows us to efficiently carve out the essence of various limit regimes for atmospheric flows without having to go through the details of the asymptotic expansions. **Figure 1** summarizes the mid-latitude flow regimes discussed in this way below.

The classical Strouhal, Mach, Froude, and Rossby numbers are now related to ε and the spatiotemporal scaling exponents via

$$\mathrm{St}^{-1} = \frac{L}{UT} = \frac{\varepsilon^{\alpha_t}}{\varepsilon^{\alpha_x}}, \quad \mathrm{Fr}^2 = \gamma \mathrm{Ma}^2 = \frac{\gamma U^2}{C^2} = \varepsilon^3, \quad \mathrm{Ro} = \varepsilon^{\alpha_x - 1}, \tag{10}$$

where T, L, U, and C are the characteristic timescale and length scale, horizontal flow velocity, and sound speed in the rescaled variables from Equations 8 and 9, respectively.

1.4. Remarks

We restrict the discussion here to length scales larger or equal to the density scale height. Of course, on length scales and timescales comparable with those of typical engineering applications, turbulence will induce a continuous range of scales. Analyses that exclusively rely on the assumption of scale separations are of limited value in studying such flows. The interested reader may want to consult Oberlack (2006) for theoretical foundations and references.

Some researchers (e.g., see White 2002, section 9.3) would not necessarily agree that formal asymptotics as promoted here is the best way forward in developing approximate model equations for atmospheric-flow applications. Salmon (1998) and Norbury & Roulstone (2002) provide excellent starting points for the interested reader.

Other researchers (e.g., Lovejoy & Schertzer 1986, Lovejoy et al. 2008) would dispute our basic proposition that a natural scale separation exists for atmospheric flows of sufficiently large scale. Their arguments are based on the difficulty of detecting such scale separations in the observational record. In response, we refer readers to our discussion above, and to Lundgren (1982) or Hunt & Vassilicos (1991). These authors demonstrate that some localized (i.e., ideally scale-separated) and entirely realizable flow structures exhibit full spectra without gaps and with exponents akin to those of turbulence spectra. In other words, there may very well be clean scale separations even if they are not visible in spectral decompositions.

2. SINGLE-SCALE REGIMES

Here we summarize the hierarchy of models that can be obtained from Equation 9 when we assume that solutions depend on a single horizontal, a single vertical, and a single timescale only. These models encapsulate the essential physical processes that interact in the multiple-scales regimes discussed in Section 3 below.

There is common agreement among meteorologists that, on length scales small compared with the planetary scale, acoustic modes contribute negligibly little to the atmospheric dynamics. As a consequence, there has been long-standing interest in analogs to the classical incompressible flow equations that would be valid for meteorological applications. Such models would capture the effects of advection, vertical stratification, and of the Coriolis force, while discarding acoustic modes.

According to our discussion above, given a horizontal characteristic length, acoustic waves, internal waves, and advection are all associated with their individual characteristic timescales. Therefore, after deciding to eliminate the sound waves, we still have the option of adjusting a reduced model to the internal wave dynamics (Section 2.1) or to capture the effects of advection (Section 2.2).

2.1. Mid-Latitude Internal Gravity Wave Models

Here we consider Equation 9 with $\alpha_t = \alpha_x - 1$, so that temporal variations are fast compared with trends due to advection, and we restrict ourselves to length scales up to the synoptic scale, $L_{\mathrm{Ro}} = h_{\mathrm{sc}}/\varepsilon^2$, so that $\alpha_x \in \{0, 1, 2\}$. The resulting leading-order models include the time derivative at $O(1/\varepsilon)$ but not the advection terms. The Coriolis terms do not dominate the time derivative unless $\alpha_x > 2$. As a consequence, for any horizontal scale $L \leq h_{\mathrm{sc}}/\varepsilon^2$, the level of pressure perturbations can be assessed from the horizontal momentum equation (Equation 9a) by balancing the pressure gradient and time-derivative terms, and we find $\alpha_\pi = 2$. With this information at hand, we observe that the velocity divergence term dominates the pressure equation (Equation 9c) so that a divergence constraint arises at leading order. From these observations, we obtain a generic leading-order model for horizontal scales $h_{\mathrm{sc}} \leq L \leq h_{\mathrm{sc}}/\varepsilon^2 = L_{\mathrm{Ro}}$,

$$\frac{\partial \boldsymbol{v}_{\|}}{\partial \tau} + af\boldsymbol{k} \times v_{\|} + \nabla_\xi \tilde{\pi} = Q^{\varepsilon}_{v_{\|}}, \tag{11a}$$

$$b\frac{\partial \tilde{w}}{\partial \tau} + \frac{\partial \tilde{\pi}}{\partial z} = \tilde{\theta}, \tag{11b}$$

$$\nabla \cdot (\bar{P} v) = 0, \tag{11c}$$

$$\frac{\partial \tilde{\theta}}{\partial \tau} + \tilde{w}\frac{d\bar{\theta}}{dz} = Q^{\varepsilon}_{\Theta}. \tag{11d}$$

Here we introduce the vertical component of Earth's rotation vector, $f = \boldsymbol{k} \cdot 2\boldsymbol{\Omega}$, with $\boldsymbol{k}$ the vertical unit vector, and we abbreviate

Geostrophic balance: pressure gradient balancing the Coriolis force

$$\nabla \cdot (\bar{P}\boldsymbol{v}) = \bar{P}\left(\nabla_{\boldsymbol{\xi}} \cdot \boldsymbol{v}_{||} + \frac{\partial \tilde{w}}{\partial z} + \frac{\tilde{w}}{\gamma \Gamma \pi}\frac{d\bar{\pi}}{dz}\right),$$

where $\bar{P}(z) = \bar{\pi}(z)^{1/\gamma\Gamma} = \bar{p}^{1/\gamma}$. The parameters a and b in Equation 11 depend on the characteristic horizontal scale and are defined as

$$a = \begin{cases} 1 & (\alpha_x = 2) \\ 0 & (\alpha_x \in \{0, 1\}) \end{cases}, \quad b = \begin{cases} 1 & (\alpha_x = 0) \\ 0 & (\alpha_x \in \{1, 2\}) \end{cases}. \tag{12}$$

For any pair (a, b), the model equations in Equation 11 are soundproof because of the velocity divergence constraint (Equation 11c). They support internal gravity waves through the interplay of vertical advection of the background stratification in Equation 11d and the buoyancy force on the right-hand side of the vertical momentum equation (Equation 11b). When $b = 0$ (i.e., for horizontal scales $L \gg h_{\mathrm{sc}}$), we have $\partial\bar{\pi}/\partial z = \tilde{\theta}$, and these waves are called hydrostatic; for $b = 1$ they are nonhydrostatic with the inertia of the vertical motion participating in the dynamics.

When $a = 0$ (i.e., for length scales small compared with the synoptic scale, $L_{\mathrm{Ro}} \sim h_{\mathrm{sc}}/\varepsilon^2$), the internal waves propagate freely. Hydrostatic states at rest with horizontally homogeneous $\tilde{\theta}$ are then the only equilibrium states of the system. For length scales comparable with the synoptic scale, however, $a = 1$, and the Coriolis effect influences the dynamics. As a consequence, there are new nontrivial steady states involving the geostrophic balance of the Coriolis and horizontal pressure gradient terms, i.e., $f\boldsymbol{k} \times \boldsymbol{v}_{||} + \nabla_{\boldsymbol{\xi}}\tilde{\pi} = 0$. Instead of assuming hydrostatic states at rest, such a system adjusts to the geostrophic state compatible with its initial data over long times, and it generally releases only a fraction of the full potential energy that it held initially (see Gill 1982, chapter 7).

In the lower part of **Figure 2** we see an internal wave train set off by the flow of a stably stratified layer of air over a mountain of height ~600 m and characteristic width ~1 km. The figure shows how the level sets of potential temperature are distorted by the vertical displacements induced by the gravity wave. We discuss other aspects of **Figure 2** in Section 2.3.

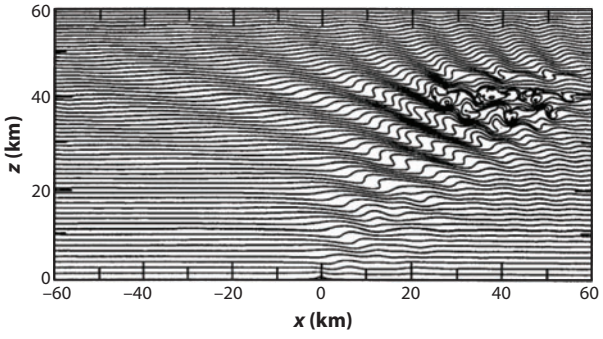

Figure 2

Internal waves triggered by flow over a single mountain visualized by level sets of the potential temperature. High up in the atmosphere, the disturbances amplify so that nonlinear effects become important and the waves break due to overturning. Figure adapted from Smolarkiewicz & Margolin 1997, their figure 4b.

2.2. Balanced Models for Advection Timescales

Here we let $\alpha_t = \alpha_x$ in Equation 9; i.e., we consider processes that always include the effects of advection in their temporal evolution. Now we have to distinguish between the meso-scales, $L = h_{\mathrm{sc}}$ and $L = L_{\mathrm{meso}} = h_{\mathrm{sc}}/\varepsilon$, on the one hand, and the synoptic scale, $L = L_{\mathrm{Ro}} = h_{\mathrm{sc}}/\varepsilon^2$, on the other hand. For the latter, the Coriolis term becomes asymptotically dominant.

2.2.1. Weak-temperature-gradient models for the meso-scales. On the meso-scales, i.e., for $\alpha_x \in \{0, 1\}$, the horizontal momentum balance in Equation 9a yields $\alpha_\pi = 3$, and we find the weak-temperature-gradient or quasi-nondivergent approximation at leading order,

$$\left(\frac{\partial}{\partial\tau} + \boldsymbol{v}_{||}\cdot\nabla_\xi + \tilde{w}\frac{\partial}{\partial z}\right)\boldsymbol{v}_{||} + af\boldsymbol{k}\times\boldsymbol{v}_{||} + \nabla_\xi\tilde{\pi} = \boldsymbol{Q}^{\varepsilon}_{v_{||}}, \tag{13a}$$

$$\nabla\cdot(\bar{\rho}\boldsymbol{v}) = 0, \tag{13b}$$

$$\tilde{w}\frac{d\bar{\theta}}{dz} = Q^{\varepsilon}_{\Theta}, \tag{13c}$$

where $a = 0$ for $L = h_{\mathrm{sc}}$, and $a = 1$ for $L = h_{\mathrm{sc}}/\varepsilon = L_{\mathrm{meso}}$ (Held & Hoskins 1985, Sobel et al. 2001, Zeytounian 1990).

Equation 13c describes how diabatic heating in a sufficiently strongly stratified medium induces vertical motions so that air parcels adjust quasi-statically to their individual vertical levels of neutral buoyancy. Replacing the potential-temperature transport equation from Equation 9d with Equation 13c suppresses internal gravity waves, just as the divergence constraints suppress the acoustic modes. With Equation 13c, the vertical velocity is fixed, given the diabatic source term. The second equation then becomes a divergence constraint for the horizontal velocity, and the perturbation pressure $\tilde{\pi}$ is responsible for guaranteeing compliance with this constraint. The vertical momentum equation (Equation 9b) in this regime becomes the determining equation for potential-temperature perturbations, $\tilde{\theta}$. These are passive unless they influence the source terms in Equation 13.

Weak-temperature-gradient models are frequently employed for studies in tropical meteorology (see Bretherton & Sobel 2001, Majda & Klein 2003, Shaevitz & Sobel 2004, and the papers in Klein 2006; see also Gill 1982, Zeytounian 1990 for detailed derivations).

2.2.2. Synoptic scales and the quasi-geostrophic approximation. On the larger synoptic length scale and advective timescales, $L = h_{\mathrm{sc}}/\varepsilon^2 \sim 1100$ km and $T = h_{\mathrm{sc}}/\varepsilon^2 u_{\mathrm{ref}} \sim 12$ h, respectively, for which $\alpha_t = \alpha_x = 2$, we find that the Coriolis and pressure gradient terms form the geostrophic balance at leading order, and this changes the dynamics profoundly in comparison with the weak-temperature-gradient dynamics from the last section. Here we encounter the likely most-prominent classical model of theoretical meteorology, the quasi-geostrophic model (see Gill 1982, Pedlosky 1987, Zeytounian 1990, and references therein; see also Muraki et al. 1999 for a higher-order accurate quasi-geostrophic theory).

Matching the Coriolis and pressure gradient terms, which are $O(\varepsilon^{-1})$ and $O(\varepsilon^{\alpha_\pi - 3})$, provides $\alpha_\pi = 2$. The horizontal and vertical momentum equations reduce to the geostrophic and hydrostatic balances, respectively, i.e.,

$$f_0\boldsymbol{k}\times\boldsymbol{v}_{||} + \nabla_\xi\tilde{\pi} = 0, \tag{14a}$$

$$\frac{\partial\tilde{\pi}}{\partial z} = \tilde{\theta}, \tag{14b}$$

where $f_0 = \boldsymbol{k} \cdot 2\Omega|_{\xi=0}$. By taking the curl of Equation 14a and inserting Equation 14b, we obtain

$$f_0 \begin{pmatrix} -\partial v/\partial z \\ \partial u/\partial z \\ \nabla_\xi \cdot \boldsymbol{v}_{||} \end{pmatrix} = \begin{pmatrix} -\partial^2 \tilde{\pi}/\partial z \partial \eta \\ \partial^2 \tilde{\pi}/\partial z \partial \xi \\ 0 \end{pmatrix} = \begin{pmatrix} -\partial \tilde{\theta}/\partial \eta \\ \partial \tilde{\theta}/\partial \xi \\ 0 \end{pmatrix}, \tag{15}$$

Potential vorticity: scalar product of vorticity and potential-temperature gradient, divided by density, $\rho^{-1} \nabla\Theta \cdot \nabla \times \boldsymbol{v}$; (magically) preserved along pathlines in the adiabatic flow of an inviscid fluid

with ξ and η the east and northward components of $\boldsymbol{\xi}$, respectively. The first two components in Equation 15 represent the thermal wind relation introduced Section 1 and used in **Table 2** to define the universal reference flow velocity, u_{ref}. The third component in Equation 15 states that the horizontal flow is divergence-free at leading order, so that $\tilde{\pi}$ may be considered a stream function for the horizontal flow according to Equation 14a.

Equation 14 does not allow us to determine the temporal evolution of the flow. An evolution equation is obtained by going to the next order in ε and eliminating the arising higher-order perturbation functions using the vertical momentum, pressure, and potential-temperature equations (see Pedlosky 1987, section 6.5). As one may have expected, the result is a vorticity transport equation, and one finds

$$\left(\frac{\partial}{\partial \tau} + \boldsymbol{v}_{||} \cdot \nabla_\xi \right) q = Q_q^e, \tag{16}$$

where

$$q = \zeta + \beta\eta + \frac{f}{\bar{\rho}} \frac{\partial}{\partial z} \left(\frac{\bar{\rho}\tilde{\theta}}{d\bar{\theta}/dz} \right) \tag{17}$$

is the leading-order potential vorticity with ζ, β, and η defined through

$$\zeta = \boldsymbol{k} \cdot \nabla_\xi \times \boldsymbol{v}_{||}, \quad \eta = \boldsymbol{\xi} \cdot \boldsymbol{e}^{\text{north}}, \quad \boldsymbol{k} \cdot 2\boldsymbol{\Omega} = f + \beta\eta. \tag{18}$$

Thus ζ is the vertical component of vorticity, η the northward component of $\boldsymbol{\xi}$, and β the derivative of the Coriolis parameter with respect to η. The last term in Equation 17 captures the effect on vorticity of the vertical stretching of a column of air induced by nonzero first-order horizontal divergences and the constraint of mass continuity. The potential vorticity source term, Q_q^e, in Equation 16 is a combination of the heat and momentum source terms and their gradients.

Using the geostrophic and hydrostatic balances in Equation 14, the definition of potential vorticity in Equation 17 becomes

$$q = \nabla_\xi^2 \tilde{\pi} + \beta\eta + \frac{f}{\bar{\rho}} \frac{\partial}{\partial z} \left(\frac{\bar{\rho}}{d\bar{\theta}/dz} \frac{\partial \tilde{\pi}}{\partial z} \right). \tag{19}$$

This, together with Equation 14a, reveals that the transport equation from Equation 16 is a closed equation for the perturbation pressure field, $\tilde{\pi}$, given appropriate definitions of the source terms and boundary conditions.

The interpretation of the potential vorticity transport equation in Equation 16 is as follows: Total vorticity is advected along (horizontal) pathlines of the leading-order flow. In the process, vertical vorticity, ζ, adjusts to compensate for local changes of the planetary rotation, $\beta\eta$, when there are northward or southward excursions, and feels the effects of vortex stretching as captured by the third term on the right-hand side in Equation 19. Important manifestations of these processes are planetary-scale meandering motions, the Rossby waves, and baroclinic instabilities that induce the sequence of cyclones and anticyclones that constitute much of the weather statistics in the middle latitudes (see **Figure 3**) (for a comprehensive discussion, see Pedlosky 1987, chapter 7). Importantly, in the quasi-geostrophic theory, both acoustic and internal gravity waves are asymptotically filtered out, as the characteristic timescale considered is that of advection only.

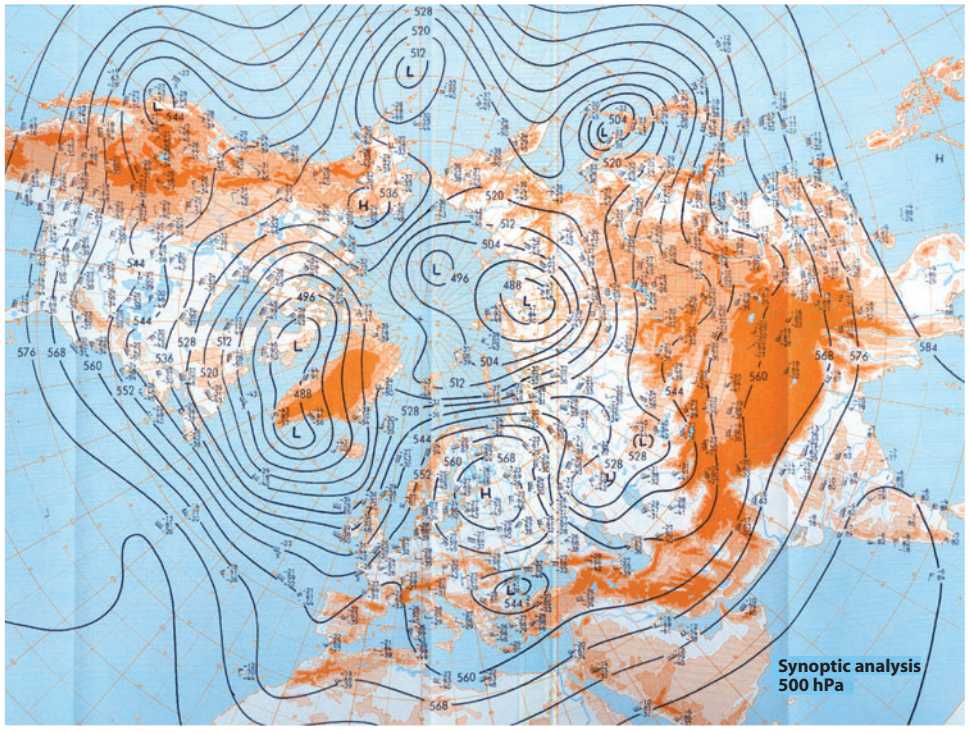

Figure 3

Chart of contours of constant geopotential height on a constant pressure surface, revealing the typical high- and low-pressure patterns known from mid-latitude weather forecasts. The associated cyclonic and anticyclonic motions are in approximate geostrophic balance, and winds are approximately directed along the contour lines. Figure courtesy of P. Névir, Meteorology, Freie Universität Berlin.

2.3. Ogura & Phillips' Anelastic Model for Weak Stratification

Above we face the choice of adopting either the internal wave or the advection timescale in constructing reduced single-scale models. A compact description of the combined effects of both would not transpire. Ogura & Phillips (1962) realized that this separation may be overcome for weak stratification and diabatic heating. To summarize their development, we let $(\bar{\theta}, Q^{\varepsilon}_{\Theta}) = \varepsilon^2(\bar{\theta}^*, Q^*_{\Theta}) = O(\varepsilon^2)$ in Equation 9d but otherwise follow the developments for the advective timescale in Section 2.2.1. With these scalings, the characteristic frequency of short internal waves, the buoyancy or Brunt-Väisälä frequency $N = \sqrt{(g/\theta)(d\theta/dz)}$, becomes comparable with the inverse of a typical advection timescale, $t^{-1}_{\mathrm{ref}} = u_{\mathrm{ref}}/b_{\mathrm{sc}}$. Equivalently, $c_{\mathrm{int}} = O(u_{\mathrm{ref}})$ as $\varepsilon \to 0$. The resulting leading-order equations constitute the classical anelastic model, and they incorporate both advection and internal wave dynamics,

$$\left(\frac{\partial}{\partial\tau} + \boldsymbol{v}_{||}\cdot\nabla_{\boldsymbol{\xi}} + \tilde{w}\frac{\partial}{\partial z}\right)\boldsymbol{v}_{||} + \nabla_{\boldsymbol{\xi}}\tilde{\pi} = \boldsymbol{Q}^{\varepsilon}_{\boldsymbol{v}_{||}}, \tag{20a}$$

$$\left(\frac{\partial}{\partial\tau} + \boldsymbol{v}_{||}\cdot\nabla_{\boldsymbol{\xi}} + \tilde{w}\frac{\partial}{\partial z}\right)\tilde{w} + \frac{\partial\tilde{\pi}}{\partial z} = \tilde{\theta} + Q^{\varepsilon}_{w}, \tag{20b}$$

$$\nabla\cdot(\bar{P}\boldsymbol{v}) = 0, \tag{20c}$$

$$\left(\frac{\partial}{\partial\tau} + \boldsymbol{v}_{||}\cdot\nabla_{\boldsymbol{\xi}} + \tilde{w}\frac{\partial}{\partial z}\right)\tilde{\theta} + \tilde{w}\frac{d\bar{\theta}^*}{dz} = Q^*_{\Theta}. \tag{20d}$$

Brunt-Väisälä or buoyancy frequency: oscillation frequency of a small air parcel in a stably stratified atmosphere, $N = \sqrt{gd\ln\Theta/dz}$

The velocity divergence constraint in Equation 20c is responsible for suppressing sound waves. For the present weak variations of potential temperature, it is equivalent to the more common formulation $\nabla \cdot (\bar{\rho}\boldsymbol{v}) = 0$ (see the definition of Θ below Equation 5). The model involves a Boussinesq-type approximation for buoyancy in Equation 20b, and the buoyancy evolution equation (Equation 20d) accounts explicitly for the background stratification. As a consequence, the system does support both internal gravity waves and the nonlinear effects of advection.

Figure 2 shows the result of Smolarkiewicz & Margolin's (1997) computational simulation of the flow over a hill based on a similar anelastic model. In the lower part of the figure, we see smooth wavelike distortions of the potential-temperature level sets, as discussed in Section 2.1 above. Energy conservation together with the strong decrease of the background density require that the velocity and potential-temperature perturbation amplitudes must continue to increase as the waves rise up in the atmosphere. Ultimately, the waves overturn, heavier air is advected nonlinearly on top of lighter air, and a strong instability induces turbulence-like fluctuations.

The total variation of potential temperature allowed for in Ogura & Phillips' anelastic model is of order $O(\varepsilon^3) = O(\mathrm{Ma}^2) \sim 10^{-3}$ [see Equations 8 and 10 and let $\bar{\theta} = O(\varepsilon^2)$]. This amounts to temperature variations of merely a few Kelvin in dimensional terms. This contrasts with the observed variations of 30. . .50 K across the troposphere. To address this issue, investigators have proposed various generalizations of the classical anelastic model allowing for stronger stratifications (e.g., see Bannon 1996, Durran 1989, Lipps & Hemler 1982). We return to this issue in Section 4.3.

2.4. Scalings for Near-Equatorial Motions

In the tropics, the same processes as encountered above contribute to the atmospheric fluid dynamics (i.e., advection, inertial effects due to the Coriolis force, and internal gravity and sound waves). However, because the Coriolis force for the horizontal motion changes sign (and is zero) at the equator, the tropical dynamics exhibit a range of different phenomena as compared with middle- and high-latitude motions. There is, in particular, a spectrum of near-equatorial trapped waves that combines aspects of internal gravity and Rossby waves and that moves predominantly in the zonal direction along the equator.

For the asymptotic scaling in ε of the Coriolis term in the horizontal momentum balance near the equator, we have $(2\boldsymbol{\Omega} \times \boldsymbol{v})_{||} = f\boldsymbol{k} \times \boldsymbol{v}_{||} + w2\boldsymbol{\Omega}_{||} \times \boldsymbol{k}$, where $f = 2\boldsymbol{\Omega} \cdot \boldsymbol{k} = 2\Omega \sin(\phi) = 2\Omega\phi + O(\phi^3)$ for small latitudes, $\phi \ll 1$. For scales smaller than the planetary scale, we place our coordinate system onto the equator and let the space coordinate y point to the north. Then, as y is nondimensionalized by $h_{\mathrm{sc}} = \varepsilon^3 a$, we have $\phi = \varepsilon^3 y$ and in Equation 9a find

$$\varepsilon(2\boldsymbol{\Omega} \times \boldsymbol{v})_{||} = \varepsilon^4 y 2\Omega\boldsymbol{k} \times \boldsymbol{v}_{||} + O(\varepsilon w). \tag{21}$$

For spatiotemporal scales that are too small for the Coriolis effect to play a leading-order role, we find essentially the same small-scale equations discussed in Section 2.1 for internal waves and in Section 2.2 for the balanced weak-temperature-gradient flows, except that the Coriolis parameter is a linear function of the meridional coordinate.

A prominent difference between tropical and mid-latitude dynamics arises at the equatorial synoptic scales, i.e., at horizontal spatial scales for which the Coriolis term again dominates the advection terms in the momentum balance even under the equatorial scaling from Equation 21. We find the governing equations for a variety of dispersive combined internal-inertial waves that are confined to the near-equatorial region and, on longer timescales, a geostrophically balanced model relevant to the tropics.

In analogy with our discussion of the scales in **Table 3**, we assess the equatorial synoptic scale, L_{es}, by equating the time an internal gravity wave would need to pass this characteristic distance

with the inverse of the Coriolis parameter. The latter, however, is now proportional to the scale we are interested in, and we obtain in dimensional terms $c_{\mathrm{int}}/L_{\mathrm{es}} = L_{\mathrm{es}}\Omega/a$, i.e., $L_{\mathrm{es}} \sim \sqrt{c_{\mathrm{int}}\, a/\Omega}$. Using Equations 1 through 3, we recover the scaling developed by Majda & Klein (2003):

$$\frac{L_{\mathrm{es}}}{h_{\mathrm{sc}}} \sim \sqrt{\frac{c_{\mathrm{ref}}}{\Omega a}\frac{c_{\mathrm{int}}}{c_{\mathrm{ref}}}\frac{a}{h_{\mathrm{sc}}}} \sim \varepsilon^{-\frac{5}{2}}. \tag{22}$$

Comparing this with Equation 4, we observe that the equatorial synoptic scale matches the asymptotic scaling of the mid-latitude Obukhov or external Rossby radius, and this corresponds to an intriguing connection between baroclinic near-equatorial waves and barotropic mid-latitude modes discussed by Majda & Biello (2003), Wang & Xie (1996).

2.5. Equatorial Subsynoptic Flow Models

For scales smaller than the equatorial synoptic scale with $L \sim h_{\mathrm{sc}}/\varepsilon^2$ or smaller, the situation is similar to that encountered for subsynoptic scales in the mid-latitudes. On the internal wave timescale, the leading-order model is again that of internal wave motions without the influence of the Coriolis force, as in Section 2.1. On advective timescales, weak-temperature-gradient models are recovered in analogy with those found in Section 2.2.1, yet with a nonconstant Coriolis parameter $f = 2\Omega\eta$ (for related derivations, see Browning et al. 2000, Majda & Klein 2003, Sobel et al. 2001). When the zonal characteristic length is allowed to be large compared with the meridional one, then a modified set of equations is obtained that still retains the advection of zonal momentum, but that is geostrophically balanced in the meridional direction (Majda & Klein 2003). We omit listing all these equations here as they are easily obtained from those in Section 2.2.1 taking into account the equatorial representation of the Coriolis term in Equation 21.

2.6. Equatorial Synoptic and Planetary Models

In the tropics, there is a strong anisotropy between the zonal and meridional directions due to the variation of the Coriolis parameter. Here we distinguish the zonal and meridional velocity components (u and v, respectively) so that $\boldsymbol{v}_{||} = u\boldsymbol{i} + v\boldsymbol{j}$. In the meridional direction, we allow for waves extending over the equatorial synoptic distance, L_{es}, whereas in the zonal direction, we have $L_x = L_{\mathrm{es}}$ for synoptic-scale waves, but $L_x \sim L_{\mathrm{es}}/\varepsilon$ for equatorial long waves (Majda & Klein 2003). Just as we scaled the vertical velocity with the vertical-to-horizontal aspect ratio before, we rescale the meridional velocity here with the meridional-to-zonal aspect ratio; i.e., we let $\eta = \varepsilon^{5/2}y$ throughout this section, but $v = \varepsilon^{\alpha_v}\tilde{v}$, with $\alpha_v = 0$ for synoptic-scale waves and $\alpha_v = 1$ for equatorial long waves. Also, we focus on the internal wave or advection timescale, so that $\alpha_t = \alpha_x - 1$ or $\alpha_t = \alpha_x$, respectively, with $\alpha_x \in \{5/2,\ 7/2\}$. In the usual way, the pressure scaling is found by balancing the dominant terms in the (zonal) momentum equation, and we have $\alpha_\pi = 2$. These scalings yield the generalized linear equatorial (wave) equations

$$\begin{aligned}
&b\frac{\partial u}{\partial \tau} - 2\Omega\eta\tilde{v} + \frac{\partial \tilde{\pi}}{\partial \xi} = \boldsymbol{Q}^{\varepsilon}_{u},\\
&ba\frac{\partial \tilde{v}}{\partial \tau} + 2\Omega\eta u + \frac{\partial \tilde{\pi}}{\partial \eta} = \boldsymbol{Q}^{\varepsilon}_{\tilde{v}},\\
&\frac{\partial \tilde{\pi}}{\partial z} = \tilde{\theta},\\
&\nabla\cdot(\bar{P}\boldsymbol{v}) = 0,\\
&b\frac{\partial \tilde{\theta}}{\partial \tau} + \tilde{w}\frac{d\tilde{\theta}}{dz} = Q^{\varepsilon}_{\Theta}.
\end{aligned} \tag{23}$$

For synoptic-scale waves with isotropic scaling in the horizontal directions, $a = 1$, whereas for equatorial long waves, there is geostrophic balance in the meridional direction and $a = 0$. To describe processes advancing on the slower advection timescale, $b = 0$, and we obtain the Matsuno-Webster-Gill model for geostrophically balanced near-equatorial motions (Matsuno 1966).

Equation 23 supports, for $b \neq 0$, a rich family of essentially different traveling waves (Gill 1982, Majda 2002, Pedlosky 1987, Wheeler & Kiladis 1999). There are fast equatorially trapped internal gravity waves that correspond to the mid-latitude internal waves from Section 2.1; slowly westward moving equatorially trapped Rossby waves; the Yanai waves, which are special solutions behaving similar to internal gravity waves at short wavelengths but similar to Rossby waves in the long wavelength limit; and finally Kelvin waves, which travel exclusively eastward and are associated with purely zonal motions (i.e., with $\tilde{v} \equiv 0$). **Figure 4** shows an overlay of the theoretical dispersion relations of these wave types with energy spectra extracted from observations by Wheeler & Kiladis (1999). We see that most of the wave types expected on theoretical grounds do actually materialize in the tropical atmosphere (see also Section 3.1 for further discussion of **Figure 4**).

In the quasi-steady balanced case, $b = 0$, Equation 23 reduces to a linear model for the geostrophically balanced flow for which exact solutions are available, given the source terms $Q^{\varepsilon}_{[\cdot]}$ (e.g., see Majda & Klein 2003, Matsuno 1966). These exact solutions are determined, however,

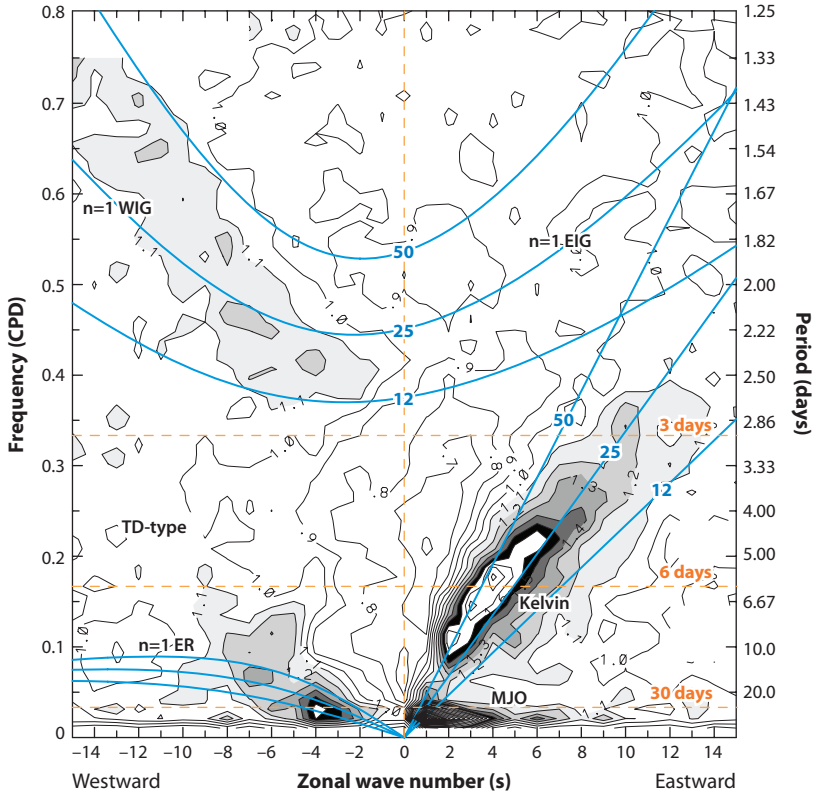

Figure 4

Dispersion diagram for equatorial shallow-water wave modes with varying equivalent depths superimposed over the contour lines of observed fluctuation intensities in the wave-number frequency domain. Figure adapted from Wheeler & Kiladis 1999, their figure 3b.

only up to a purely zonal, i.e., x-independent mean flow. Such a mean flow must either be prescribed or obtained from an analysis of the next larger zonal scale (see Majda & Klein 2003, and Section 3.1 below). The mathematical character of near-equatorial geostrophically balanced flows differs considerably from that of their mid-latitude analogs from Section 2.2.2.

2.7. The Hydrostatic Primitive Equations

In the construction of computational global weather forecasting or climate models, it is important that the basic fluid flow model used is uniformly valid on the entire globe and for the most extreme flow conditions found. The large-scale model equations discussed above are adapted to either the middle latitudes or the near-equatorial region. At the same time, one observes relatively large mean flow velocities of the order of $|\boldsymbol{v}| \sim 50\ \mathrm{m\ s^{-1}}$, corresponding to Mach numbers $\mathrm{Ma} \sim 0.15$ in strong jet streams near the tropopause (e.g., see Schneider 2006), and it turns out that global-scale barotropic wave perturbations may be equally considered as external gravity or as planetary sound waves.

These observations lead us to consider fully compressible flows with Mach numbers of order unity on horizontal scales that are large compared with the scale height, h_{sc}. Going back to our general rescaled compressible flow equations, we nondimensionalize the flow velocity by the sound speed c_{ref} instead of by u_{ref}, recalling that $u_{\mathrm{ref}}/c_{\mathrm{ref}} = \mathrm{Ma} \sim \varepsilon^{\frac{3}{2}}$ according to Equation 2. Then we let

$$\hat{\boldsymbol{v}}_{||} = \varepsilon^{\frac{3}{2}} \boldsymbol{v}_{||}, \quad \alpha_x \in \left\{1, \ldots, \frac{5}{2}\right\}, \quad \alpha_t = \alpha_x - \frac{3}{2} \tag{24}$$

and obtain, after reverting to the variables p, ρ, $\hat{\boldsymbol{v}}_{\|}$, and $\hat{w}$, and dropping the hats for convenience of notation,

$$\left(\frac{\partial}{\partial t} + \boldsymbol{v}_{||} \cdot \nabla_{\boldsymbol{\xi}} + w \frac{\partial}{\partial z}\right) \boldsymbol{v}_{||} + a f \boldsymbol{k} \times \boldsymbol{v} + \frac{1}{\rho} \nabla_{\boldsymbol{\xi}} p = Q_{v_{||}}, \tag{25a}$$

$$\frac{1}{\rho} \frac{\partial p}{\partial z} = -1, \tag{25b}$$

$$\left(\frac{\partial}{\partial t} + \boldsymbol{v}_{||} \cdot \nabla_{\boldsymbol{\xi}} + w \frac{\partial}{\partial z}\right) \rho + \rho \nabla \cdot \boldsymbol{v} = 0, \tag{25c}$$

$$\left(\frac{\partial}{\partial t} + \boldsymbol{v}_{||} \cdot \nabla_{\boldsymbol{\xi}} + w \frac{\partial}{\partial z}\right) \Theta = Q_{\Theta}, \tag{25d}$$

where $f = 2\boldsymbol{\Omega} \cdot \boldsymbol{k}$ is the vertical component of Earth's rotation vector, and $a = 0$ for $\alpha_x < 5/2$, whereas $a = 1$ for $\alpha_x = 5/2$.

The only approximations relative to the full compressible flow equations from Equation 5 result from the hydrostatic approximation for the pressure in Equation 25b; from the neglect of higher-order contributions to the Coriolis terms both in the vertical and horizontal momentum balances, i.e., from the traditional approximation (e.g., see White 2002); and possibly from our assumption regarding the nondominance of the source terms $Q_{[\cdot]}$.

The main consequence of the hydrostatic approximation is that the vertical velocity becomes a diagnostic variable that can be determined from the horizontal velocity, pressure, and potential-temperature fields at any given time by integrating a second-order ordinary differential equation in z. This can be demonstrated, e.g., by differentiating Equation 25b with respect to time and collecting all expressions involving $\hat{w}$. A more elegant way to reveal the diagnostic nature of vertical velocity is to move to pressure coordinates, i.e., to introduce the time-dependent coordinate transformation $(t, \boldsymbol{\xi}, z) \to (t, \boldsymbol{\xi}, p)$, where the transformation rule is given by the hydrostatic

relation in Equation 25b. After this transformation, one obtains a divergence constraint

$$\nabla_{\boldsymbol{\xi}}^{p}\hat{\boldsymbol{v}}_{||}+\frac{\partial\omega}{\partial p}=0, \tag{26}$$

where $\omega = Dp/Dt$ is the analog of vertical velocity in the pressure coordinates (e.g., see Salmon 1998, White 2002).

The traditional approximation for the Coriolis terms results automatically from the present asymptotic considerations. At the same time, it is extremely important for energetic reasons: Unless the traditional approximation is introduced together with the hydrostatic one, the resulting equations will not feature an energy-conservation principle, and this would render them useless for long-term integrations (White 2002).

In terms of physical processes represented, the hydrostatic primitive equations cover advection, hydrostatic internal gravity waves, baroclinic and barotropic inertial (Rossby) waves, and barotropic large-scale external gravity waves, which are the remnant of compressibility in this system and may thus equivalently be considered as its sound waves. Because the Coriolis term does not become dominant in Equation 25, there is no degeneration of these equations near the equator, and the equatorial region is represented with uniform accuracy.

The hydrostatic primitive equations form the fluid dynamical basis of most global weather forecasting and climate models today (e.g., see Houghton 2002, Lorenz 1967, Salmon 1998, Shaw & Shepherd 2009, Zeytounian 1990). In regional weather forecasting, they are being replaced with nonhydrostatic models (Clark et al. 2009, Koppert et al. 2009).

3. MULTIPLE-SCALES REGIMES

We assume here that the reader is familiar with the techniques of multiple-scales asymptotics (e.g., see Kevorkian & Cole 1996).

3.1. Majda & Biello's Model for the Madden Julian Oscillation

The Madden Julian oscillation (MJO) is an important recurrent weather pattern in the tropical atmosphere consisting of a planetary-scale modulated wave train of storms and precipitation events that travels around the globe in approximately 40–60 days (e.g., see Madden 2009 and its observational footprint in **Figure 4**).

Majda & Klein's (2003) multiple-scales asymptotic analysis of interactions between equatorial synoptic balanced flows (Equation 23 with $b = 0$) and equatorial long waves (Equation 23 with $a = 0, b = 1$) revealed how the vertical advective transport of momentum and potential temperature induced by diabatic source terms on synoptic scales can accumulate and drive planetary-scale long-wave modes. The underlying hypothesis in this work is that such multiscale interactions would be responsible for establishing the typical observed flow patterns associated with the MJO (see Biello & Majda 2005, and references therein). Biello and Majda tested this hypothesis by driving the synoptic-scale flow in this multiscale model with prescribed source terms, thereby mimicking the diabatic effects that would be associated with the observed cloud distributions and patterns of precipitation. The synoptic-scale flow and its nonlinear upscale fluxes to the planetary scale could then be determined analytically due to the essential linearity of the equatorial geostrophic equations. In this fashion, Biello and Majda could reproduce prominent features of the observed planetary-scale flow patterns and showed that some of these patterns are associated with nonlinear scale interactions rather than with just the effects of the large-scale averaged diabatic sources. Although this model does not self-consistently describe the MJO—for example, it cannot

predict the MJO wave speed—it nevertheless "provides both several diagnostic and predictive tests for both observations and current GCM simulations of the MJO" (Biello & Majda 2005) due to the theoretical insights that it has generated. (Here GCM refers to full-complexity general circulation models of the atmosphere and oceans.)

Majda (2007b) generalizes Majda & Klein's (2003) theory to cover a wide range of multiple timescales from the meso-scale to the planetary scale (see Majda & Klein 2003, their figure 1). He obtains a hierarchy of nonlinear scale interaction models that may be appropriate for modeling the apparent self-similarities in tropical convection patterns (Wheeler & Kiladis 1999) that feature clusters of small-scale convection and precipitation events forming superclusters, which then group together to produce the synoptic-scale driving forces accounted for by Biello & Majda (2005).

In related earlier work, Majda & Biello (2003) developed a weakly nonlinear multiscale theory for the baroclinic equatorial–barotropic mid-latitude interactions mentioned at the end of Section 2.4.

3.2. Shaw & Shepherd's Parameterization Framework

One important application of multiple-scales theories that has recently gained momentum is the development of sound bases for the parameterization, or closure, of the net effects of unresolved scales in computational atmospheric-flow models. An excellent example is the recent work by Shaw & Shepherd (2009). Burkhardt & Becker (2006) discuss the potentially detrimental effect of subgrid-scale parameterizations of effective diffusion, friction, and dissipation in global climate models that are not energetically and thermodynamically consistent. Shaw & Shepherd (2009) employ multiple-scales asymptotics to reveal how meso-scale internal wave processes (see Section 2.1 above) would cumulatively affect planetary-scale motions as described by the hydrostatic primitive equations (Section 2.7). Using a different set of ideas associated with wave-activity conservation laws developed by Shepherd (1990), they move on to derive simplified expressions for the discovered interaction terms that would allow them not to solve the meso-scale wave model in detail, as the formal multiple-scales asymptotics procedure would require, but would provide effective closures that are energetically and thermodynamically consistent.

Shaw & Shepherd restrict their framework, in this first layout, to the characteristic internal gravity wave time for the meso-scale and to the planetary acoustic timescale. There is thus great potential for the incorporation of wide-ranging results on wave–mean field interactions as developed in recent years (see Bühler 2010; Bühler & McIntyre 2005; H.V. Dosser & B.R. Sutherland, submitted manuscript; Sutherland 2006; and references therein). It is not clear, however, how the closure schemes addressing wave activities will carry over to situations in which nonlinear advection and (moist) convection play an important role on small scales.

3.3. Computational Multiscale Models

In multiscale theories, the equations governing the small scales are often too complex to be solved analytically. In such cases, numerical approximate solutions for the small scales need to be generated, and their net effect on the large scales has to be evaluated using numerical versions of the sublinear growth conditions, or of some equivalent constraints. This leads to the construction of computational multiscale methods. In this section we discuss two pertinent examples.

3.3.1. Superparameterization and heterogeneous multiscale models. It is, of course, by no means guaranteed that the fast or small-scale equations in a multiple-scales asymptotic analysis are analytically tractable. For example, in a two-scale model that involves the length scales $\ell \sim h_{sc}$ and

$L \sim h_{sc}/\varepsilon$ and covers the advective timescale h_{sc}/u_{ref} for the scale ℓ, the small-scale model would be either the weak-temperature-gradient flow equations from Section 2.2.1 or some version of the anelastic model from Section 2.3 (Klein & Majda 2006). In both cases, one will generally have to resort to numerical computation to determine the small-scale dynamics. In such a situation, the technique of multiple-scales analysis can nevertheless yield valuable guidelines regarding the reduced or averaged information that is to be extracted from the small-scale model and communicated to the large-scale equations. E & Engquist (2003) have systematized these procedures and proposed a framework for the construction of computational heterogeneous multiscale models (see also Engquist et al. 2007).

In the context of meteorological modeling, there is a related active, recent development aiming at overcoming one of the major deficiencies of today's climate models in an efficient way. Cloud distributions in the atmosphere feature a wide spectrum of length scales and timescales (Tessier et al. 1993). Therefore, it is generally not possible to even remotely resolve cloud processes in general circulation models for the climate, which feature horizontal grid sizes of 100 km or more. Grabowski (2001, 2004) proposed the superparameterization approach, which involves operating a two-dimensional cloud resolving model, based in his case on an extended version of the anelastic model from Section 2.3, within each of the climate model's grid boxes, and extracting the net effects of the small-scale processes on the large-scale flow through appropriate averaging procedures. In today's terms, the approach may be considered a heterogeneous multiscale model for cloud processes in climate applications. Majda (2007a) formulated a general framework for the construction of such hierarchies of embedded models based on the general multiple-scales approach by Klein and colleagues (Klein 2000, 2004; Majda & Klein 2003). In particular, he accounts explicitly for the existence of two more groups of characteristic length scales and timescales to be accounted for between the convective length scale of the order of h_{sc} and the planetary (climate) scale, as explained here in Section 2. In this context, we note that Nadiga et al. (1997) demonstrated the feasibility of a direct translation of multiple-scales techniques into a working computational geofluid dynamics code.

3.3.2. Synoptic-planetary interactions in the mid-latitudes. There is increasing interest in the climate and climate-impact research community to develop Earth system models of intermediate complexity (Petoukhov et al. 2000). Such models are computationally more efficient than full-fledged global circulation models (Roeckner et al. 2003), albeit they provide much coarser resolution only. They are used for long-term paleoclimate simulations and for Earth system modeling, in which case they get coupled to a wide range of additional physical, biological, and socioeconomic processes. In both settings, their computational speed is decisive for the feasibility of the modeling effort. Conversely, they have the potential to support our understanding of the climate system in an important way that is complementary to what is provided by the output of highly complex general circulation model simulations: They yield a much more direct and analytically tractable insight into the scale interactions for which they are designed to account.

Pedlosky (1984) derived an elegant mid-latitude synoptic–to–planetary scale interaction theory using techniques of multiple-scales asymptotics. The theory combines a planetary geostrophic model, attributed originally to Needler (1967), with the quasi-geostrophic theory explained in Section 2.2.2 above. This work seems widely known and is referred to mostly in the oceanographic literature, although it is, with some modifications, also applicable to atmospheric flows (Dolaptchiev 2008, Dolaptchiev & Klein 2009). It would be interesting to replace the turbulence-like closure schemes for the synoptic dynamics used by Petoukhov et al. (2000) with an analytical or computational heterogeneous multiscale closure based on these systematic results from multiple-scales analysis.

3.4. Moist Processes

Emanuel (1994) provides a comprehensive treatise of moisture-related processes in the atmosphere and of their theoretical and computational modeling. However, besides the pioneering scale analysis by Lipps & Hemler (1982, 1985), which led them to develop the famous Lipps-Hemler generalization of Ogura & Phillips' anelastic model from Section 2.3, there seem to have been no serious attempts at systematically studying the influence of the moist thermodynamics on atmospheric fluid mechanics using asymptotic methods until recently. Klein & Majda (2006) generalized Lipps & Hemler's studies in several ways. They embedded the analysis of moist flows in the general asymptotic framework described in Section 1 above. Using a bulk microphysics moisture model as proposed by Grabowski (1998) and Kessler (1969), they included appropriate distinguished limits for the dimensionless phase transition rates (Damköhler numbers) as familiar from combustion theory (Peters 2000). On this basis, they developed two multiscale models valid for (*a*) interactions between the convective or meso-γ and the meso-β scale (see **Table 3**) and (*b*) interactions between narrow but deep columns of moist saturated air that are on the verge of forming deep convective columns (see Carqué et al. 2008a,b; Majda 2007a; Majda & Xing 2009 for further developments and work in progress).

Whereas Lipps & Hemler (1982, 1985) and Klein & Majda (2006) adopted a number of simplifying assumptions regarding the complexity of the equations of state of moist air, Pauluis (2008) demonstrates that an energetically consistent version of the anelastic model can be formulated even when the full nonlinearity of the moist gas equations of state is maintained.

4. CONCLUDING THOUGHTS

4.1. Warnings and Alternative Approaches to Approximation

Formal asymptotic expansions do not automatically yield universally valid approximations. In fact, the scaling arguments given in Section 1 suggest that with every scale factor of $1/\varepsilon$ in length or time, we should expect new phenomena to enter the scene and influence the associated flow phenomena. Thus, caution voiced, e.g., by White (2002, section 9.3) in his excellent review article on model equations for atmospheric flows, is well justified. To avoid ending up with a simplified model that is applicable only over a narrow time span or spatial range, one might want to follow alternative approaches. For example, for Hamiltonian systems, Salmon (1983) proposes that we preserve the Hamiltonian structure of a system and approximate the Hamiltonian rather than ensuring asymptotic consistency to some given order in a small parameter for the governing equations. This approach guarantees long-time stability of solutions of the resulting equations, at least in the energy norm of the Hamiltonian. It does not necessarily guarantee that the solution to the approximate equations remains a good approximation to the solution of the original system over such long times (see also Névir 2004, Névir & Blender 1993, Oliver 2006, and references therein; for related developments of numerical techniques, see Cotter & Reich 2006, Gassmann & Herzog 2008).

4.2. Rigorous Justifications of Reduced Asymptotic Models

There is a rich literature on the mathematically rigorous justifications of reduced asymptotic models. The goal of these studies is to prove that, for some finite or for infinite time, a reduced model derived through formal asymptotic analysis does, in fact, produce solutions that stay close to those of the original system. This is especially challenging in multiscale systems, as one must show that the

NUMERICAL COMPUTATION OF MULTISCALE ATMOSPHERIC FLOWS

The ever-increasing power of high-performance computers leads to continuously increasing spatiotemporal resolutions in weather forecasting and climate models. Interestingly, the notion of increased resolution in both atmosphere-ocean science and the engineering discipline of large eddy simulation is orthogonal to that in mathematics. Increased resolution allows the geophysical or engineering modeler to represent a broader range of physical processes explicitly, thereby simplifying the task of subgrid-scale parameterization. In contrast, increased resolution from a mathematical perspective provides results that are closer to the ideal of a converged solution. Thus, the atmosphere-ocean scientist would naturally refine the computational grid and at the same time adjust his mathematical model, whereas the mathematician would certainly fix the mathematical model while studying convergence.

Both approaches are well founded, yet incompatible. Developing concepts that would hold up to the standards of both disciplines is a major challenge, requiring close interdisciplinary interaction and some fresh ideas that will allow us to merge analytical multiscale techniques with clean numerical approximation algorithms (see also **http://metstroem.mi.fu-berlin.de**).

[Adapted from the workshop proposal "Mathematical Theory and Modelling of Atmosphere-Ocean Flows" (A. Majda, B. Stevens & R. Klein) to be held at the Mathematics Research Institute Oberwolfach, Germany, in August 2010.]

equations for the fast time evolution have meaningful solutions over times of order $1/\varepsilon$ when ε characterizes the timescale separation. Analogous statements hold for multiple space scale problems.

Pioneering work on proofs that the incompressible flow equations yield proper approximations to flows at very low Mach numbers was developed by Ebin (1977) and Klainerman & Majda (1982). Schochet (2005) reviews work on this problem and, in particular, describes extensions of the general technical framework that allow one to simultaneously handle multiple length scales and timescales. Embid & Majda (1998a,b) and Babin et al. (2002) (see also their earlier references) developed rigorous theories that prove the validity of quasi-geostrophic approximations in various regimes for the boundary, far-field, and initial data (see also Bresch & Gérard-Varet 2007, Zeitlin 2007, and references therein, for theoretical developments on shallow-water rotating flows including the effects of short-scale topography).

Dutrifoy et al. (2009) justify the equatorial long wave equation in two space dimensions, i.e., in the shallow-water approximation. This work goes nontrivially beyond the previous cases in that, due to the meridional variation of the Coriolis parameter (see Section 2.4), the linear leading order system describing the fast modes has nonconstant coefficients. This makes it a key challenge to prove that smooth solutions will stay smooth over asymptotically long times (when measured on the fast timescale).

The studies mentioned above are valid for inviscid flows. If there is sufficient dissipation in a system, different analysis techniques that use explicitly the regularizing properties of viscosity and diffusion can be employed (see Bresch & Desjardins 2003, Levermore et al. 1996 for related work on the shallow-water equations; Cao & Titi 2003, 2007 for analyses of the hydrostatic primitive equations; and Feireisl et al. 2008, Masmoudi 2007 for justifications of the anelastic model, albeit for the case of neutral stratification that will not support internal waves).

4.3. Limits of Formal Asymptotics and an Interesting Challenge

Section 2.3 demonstrates that a reduced set of equations that is soundproof yet retains internal waves and advection on the same timescale can be derived through formal asymptotics only if

we assume exceedingly weak stratification. Derivations of extended anelastic models for stronger, realistic stratifications cannot be asymptotically consistent—unless they somehow incorporate the two asymptotically separated timescales of advection and internal waves. The derivations that I have seen (Bannon 1996; Durran 1989; Lipps & Hemler 1982, 1985) never address this issue (for further discussion, see Botta et al. 2000; Klein 2000, 2009). An interesting aspect of internal waves in this context is that they are strongly dispersive. The magnitude of their phase and group velocities varies strongly with the direction and magnitude of the wave-number vector (e.g., see Salmon 1998, chapter 7). Thus, whereas long-wavelength modes feature phase speeds comparable to c_{int} from **Table 2**, there are somewhat shorter waves with a nonzero vertical component of the phase vector that have a propagation speed comparable to merely u_{ref}. As a consequence, the extended anelastic and pseudoincompressible models are true multiscale models covering a continuous range of scales, as indicated in **Figure 1**.

The extended anelastic and pseudoincompressible models have proven to be extremely useful in a large number of studies and applicable even up to planetary scales (Wedi & Smolarkiewicz 2009). From a theoretical point of view, however, we are still faced with the interesting question of how these models represent in a precise sense approximations to the full compressible flow equations in atmospheric-flow regimes.

In the meantime, Arakawa & Konor (2009) and Durran (2008) have already moved on to propose intriguing multiscale systems of equations for global cloud-resolving simulations that combine anelastic or pseudoincompressible dynamics for the small scales with the hydrostatic primitive equations from Section 2.7 for the planetary scales. Similar questions arise here.

4.4. One More Warning

In this review I consciously address only the fluid mechanically induced scale separations and their consequences for the construction of reduced reduced-flow models. The ubiquitous source terms $Q_{[\cdot]}$ may impose additional characteristics both in terms of spatiotemporal scales and in terms of their response to variations of the flow variables. As is well-known, e.g., from combustion theory, this can strongly affect the resulting simplified models (Klein & Majda 2006, Peters 2000).

SUMMARY POINTS

1. A set of universal characteristics of Earth's atmosphere allows us to identify three small parameters that motivate a natural scale separation for length scales and timescales larger than approximately 10 km and 20 min. Physically, this scale separation is associated with three distinct characteristic signal speeds: the sound speed, the speed of internal gravity waves, and the thermal wind velocity, which incorporates the Coriolis effect.
2. For timescales long compared with a sound wave's travel time, single-scale asymptotic analyses produce fast-time internal/inertial wave models and slow-time, buoyancy-controlled weak-temperature-gradient or quasi-nondivergent approximations. On the advective timescale and synoptic length scale, the classical quasi-geostrophic theory emerges.
3. Anelastic models valid for realistic atmospheric stratifications that combine internal waves and advection in a single set of partial differential equations are inherently multiscale and are not straightforwardly derived by multiple-scales asymptotic expansions.

4. Recent developments include explicit multiple-scales theories for the MJO, for parameterizations and superparameterizations in climate models, and new theories for scale interactions in moist atmospheric flows.
5. Some reduced asymptotic models provide provably correct approximations in a mathematically rigorous sense. For other models that have proven to be extremely useful in practice, there are neither formal asymptotic derivations nor alternative mathematical arguments for their validity, although there are many physically intuitive ones. Then there are alternatives to formal asymptotic expansions in deriving approximate models, such as Hamiltonian systems with approximate Hamiltonians.

FUTURE ISSUES

1. We need to develop mathematically sound ways of representing unresolved scale processes in computational models of the atmosphere. Here mathematically sound means, in particular, also sound in the sense of numerical analysis.
2. A hierarchy of global atmosphere-ocean models should be created that would implement the various levels of approximation outlined in this review in one computational framework. This would greatly support our efforts at gaining an improved understanding of the nature of both the physical climate system and the large-scale numerical simulations currently undertaken on the basis of modern general circulation models [such as ECHAM5 (Roeckner et al. 2003)].
3. Formal and rigorous mathematical strategies should be developed for the reduction of the number of scales in systems with more than two scales (for example, see the discussion on anelastic models in Section 4.3).

DISCLOSURE STATEMENT

The author is not aware of any affiliations, memberships, funding, or financial holdings that might be perceived as affecting the objectivity of this review.

ACKNOWLEDGMENTS

The author thanks Ulrich Achatz, Dargan Frierson, Juan Pedro Mellado, Norbert Peters, Heiko Schmidt, and Bjorn Stevens for helpful discussions and suggestions concerning the content and structure of this manuscript and Ulrike Eickers for her careful proofreading.

LITERATURE CITED

Arakawa A, Konor CS. 2009. Unification of the anelastic and quasi-hydrostatic systems of equations. *Mon. Weather Rev.* 137:710–26

Babin A, Mahalov A, Nicolaenko B. 2002. Fast singular limits of stably stratified 3D Euler and Navier-Stokes equations and ageostrophic wave fronts. See Norbury & Roulstone 2002, pp. 126–201

Bannon PR. 1996. On the anelastic approximation for a compressible atmosphere. *J. Atmos. Sci.* 53:3618–28

Biello JA, Majda AJ. 2005. A new multiscale model for the Madden-Julian oscillation. *J. Atmos. Sci.* 62:1694–721

Botta N, Klein R, Almgren A. 2000. Asymptotic analysis of a dry atmosphere. In *Proc. 3rd ENUMATH, Jyväskylä, Finland 1999*, ed. P Neittaanmäki, T Tiihonen, P Tarvainen, pp. 262–71. Singapore: World Sci.

Bresch D, Desjardins B. 2003. Existence of global weak solutions for a 2D viscous shallow water equations and convergence to the quasi-geostrophic model. *Commun. Math. Phys.* 238:211–23

Bresch D, Gérard-Varet D. 2007. On some homogenization problems from shallow water theory. *Appl. Math. Lett.* 20:505–10

Bretherton C, Sobel A. 2001. The Gill model and the weak temperature gradient (WTG) approximation. *J. Atmos. Sci.* 60:451–60

Browning G, Kreiss HO, Schubert WH. 2000. The role of gravity waves in slowly varying in time tropospheric motions near the equator. *J. Atmos. Sci.* 57:4008–19

Bühler O. 2010. Wave-vortex interactions in fluids and superfluids. *Annu. Rev. Fluid. Mech.* 42: In press

Bühler O, McIntyre ME. 2005. Wave capture and wave-vortex duality. *J. Fluid Mech.* 534:67–95

Burkhardt U, Becker E. 2006. A consistent diffusion-dissipation parameterization in the ECHAM climate model. *Mon. Weather Rev.* 134:1194–204

Cao C, Titi E. 2003. Global well-posedness and finite dimensional global attractor for a 3-D planetary geostrophic viscous model. *Commun. Pure Appl. Math.* 56:198–233

Cao C, Titi E. 2007. Global well-posedness of the three-dimensional viscous primitive equations of large scale ocean and atmosphere dynamics. *Ann. Math.* 166:245–67

Carqué G, Owinoh A, Klein R, Majda AJ. 2008a. Asymptotic scale analysis of precipitating clouds. *Tech. Rep.*, Zuse Inst. Berlin, **http://opus.kobv.de/zib/volltexte/2008/1083/**

Carqué G, Schmidt H, Stevens B, Klein R. 2008b. Plausibility check of an asymptotic column model for deep convective clouds. *Tech. Rep.*, Zuse Inst. Berlin, **http://opus.kobv.de/zib/volltexte/2008/1133/**

Clark P, Hartwig E, Killeen T, Kulesa G, Lanicci J, et al. 2009. *The weather research and forecasting model*. **http://www.wrf-model.org/**

Cotter CJ, Reich S. 2006. Semigeostrophic particle motion and exponentially accurate normal forms. *SIAM J. Multiscale Mod. Simul.* 5:476–96

Dolaptchiev SI. 2008. *Asymptotic models for planetary scale atmospheric motions*. Ph.D. thesis. Freie Univ. Berlin

Dolaptchiev SI, Klein R. 2009. Planetary geostrophic equations for the atmosphere with evolution of the barotropic flow. *Dyn. Atmos. Oceans* 46:46–61

Durran DR. 1989. Improving the anelastic approximation. *J. Atmos. Sci.* 46:1453–61

Durran DR. 2008. A physically motivated approach for filtering acoustic waves from the equations governing compressible stratified flow. *J. Fluid Mech.* 601:365–79

Dutrifoy A, Schochet S, Majda AJ. 2009. A simple justification of the singular limit for equatorial shallow-water dynamics. *Commun. Pure Appl. Math.* 62:322–33

E W, Engquist B. 2003. The heterogeneous multi-scale methods. *Commun. Math. Sci.* 1:87–133

Ebin DG. 1977. The motion of slightly compressible fluids viewed as a motion with strong constraining force. *Ann. Math.* 105:141–200

Emanuel KA. 1994. *Atmospheric Convection*. New York: Oxford Univ. Press

Embid P, Majda AJ. 1998a. Averaging over fast gravity waves for geophysical flows with unbalanced initial data. *Theor. Comput. Fluid Dyn.* 11:155–69

Embid P, Majda AJ. 1998b. Low Froude number limiting dynamics for stably stratified flow with small or finite Rossby numbers. *Geophys. Astrophys. Fluid Dyn.* 87:1–50

Engquist B, E W, Vanden-Eijnden E. 2007. Heterogeneous multiscale methods: a review. *Commun. Comput. Phys.* 2:367–450

Feireisl E, Málek J, Novotný A, Straškraba I. 2008. Anelastic approximation as a singular limit of the compressible Navier-Stokes system. *Commun. Partial Differ. Equ.* 33:157–76

Frierson DMW. 2008. Midlatitude static stability in simple and comprehensive general circulation models. *J. Atmos. Sci.* 65:1049–62

Gassmann A, Herzog H. 2008. Towards a consistent numerical compressible non-hydrostatic model using generalized Hamiltonian tools. *Q. J. R. Meteorol. Soc.* 134:1597–613

Gill AE. 1982. *Atmosphere-Ocean Dynamics*. Int. Geophys. Ser. vol. 30. San Diego: Academic

Grabowski WW. 1998. Toward cloud resolving modeling of large-scale tropical circulations: a simple cloud microphysics parameterization. *J. Atmos. Sci.* 55:3283–98
Grabowski WW. 2001. Coupling cloud processes with the large-scale dynamics using the cloud-resolving convection parameterization (CRCP). *J. Atmos. Sci.* 58:978–97
Grabowski WW. 2004. An improved framework for superparameterization. *J. Atmos. Sci.* 61:1940–52
Held IM, Hoskins BJ. 1985. Large-scale eddies and the general circulation of the troposphere. *Adv. Geophys.* 28:3–31
Houghton J, ed. 2002. *The Physics of Atmospheres*. Cambridge, UK: Cambridge Univ. Press
Hunt JCR, Vassilicos JC. 1991. Kolmogoroff's contributions to the physical and geometrical understanding of small-scale turbulence and recent developments. *Proc. R. Soc. London A* 434:183–210
Keller J, Ting L. 1951. Approximate equations for large scale atmospheric motions. *Intern. Rep.*, Inst. Math. Mech., NYU; **http://www.arxiv.org/abs/physics/0606114v2**
Kessler E. 1969. On the distribution and continuity of water substance in atmospheric circulations. *Meteorol. Monogr.* 10:82–84
Kevorkian J, Cole J. 1996. *Multiple Scale and Singular Perturbation Methods*. New York: Springer Verlag
Klainerman S, Majda AJ. 1982. Compressible and incompressible fluids. *Commun. Pure Appl. Math.* 35:629–51
Klein R. 2000. Asymptotic analyses for atmospheric flows and the construction of asymptotically adaptive numerical methods. *Z. Angew. Math. Mech.* 80:765–77
Klein R. 2004. An applied mathematical view of theoretical meteorology. In *Applied Mathematics Entering the 21st Century: Invited Talks from the ICIAM 2003 Congress*, ed JM Hill, R Moore, pp. 177–219. SIAM Proc. Appl. Math. vol. 116. Philadelphia, PA: SIAM
Klein R, ed. 2006. Special Issue: Theoretical Developments in Tropical Meteorology. *Theor. Comp. Fluid Dyn.* 20:227–551
Klein R. 2008. An unified approach to meteorological modelling based on multiple-scales asymptotics. *Adv. Geosci.* 15:23–33
Klein R. 2009. Asymptotics, structure, and integration of sound-proof atmospheric flow equations. Theor. Comp. Fluid Dyn. In press; doi: 10.1007/s00162-009-0104-y
Klein R, Majda AJ. 2006. Systematic multiscale models for deep convection on mesoscales. *Theor. Comp. Fluid Dyn.* 20:525–52
Koppert HJ, Rotach M, Ferri M, Charantonis T, Ziemianski M, Pescaru V. 2009. *Consortium for small-scale modelling*. **http://www.cosmo-model.org/**
Levermore CD, Oliver M, Titi ES. 1996. Global well-posedness for models of shallow water in a basin with a varying bottom. *Indiana Univ. Math. J.* 45:479–510
Lipps F, Hemler R. 1982. A scale analysis of deep moist convection and some related numerical calculations. *J. Atmos. Sci.* 39:2192–210
Lipps F, Hemler R. 1985. Another look at the scale analysis of deep moist convection. *J. Atmos. Sci.* 42:1960–64
Lorenz EN. 1967. *The Nature and Theory of the General Circulation of the Atmosphere*. Geneva: World Meteorol. Org.
Lovejoy S, Schertzer D. 1986. Scale invariance, symmetries, fractals, and stochastic simulations of atmospheric phenomena. *Bull. Am. Meteorol. Soc.* 67:21–32
Lovejoy S, Tuck AF, Hovde SJ, Schertzer D. 2008. Do stable atmospheric layers exist? *Geophys. Res. Lett.* 35:L01802
Lundgren TS. 1982. Strained spiral vortex model for turbulent fine structure. *Phys. Fluids* 25:2193–203
Madden RA. 2009. *Madden-Julian oscillation life cycle*. **http://www.meted.ucar.edu/climate/mjo**
Majda AJ. 2002. *Introduction to PDEs and Waves for the Atmosphere and Ocean*. Courant Lect. Notes Vol. 9. Providence, RI: Am. Math. Soc./Courant Inst. Math. Sci.
Majda AJ. 2007a. Multiscale models with moisture and systematic strategies for superparameterization. *J. Atmos. Sci.* 64:2726–34
Majda AJ. 2007b. New multiscale models and self-similarity in tropical convection. *J. Atmos. Sci.* 64:1393–404
Majda AJ, Biello JA. 2003. The nonlinear interaction of barotropic and equatorial baroclinic Rossby waves. *J. Atmos. Sci.* 60:1809–21
Majda AJ, Klein R. 2003. Systematic multi-scale models for the tropics. *J. Atmos. Sci.* 60:393–408

Majda AJ, Xing Y. 2009. New multi-scale models on mesoscales and squall lines. *Commun. Math. Sci.* In press
Masmoudi N. 2007. Rigorous derivation of the anelastic approximation. *J. Math. Pures Appl.* 3:230–40
Matsuno T. 1966. Quasi-geostrophic motions in the equatorial area. *J. Metereol. Soc. Jap.* 44:25–43
Muraki DJ, Snyder C, Rotunno R. 1999. The next-order corrections to quasigeostrophic theory. *J. Atmos. Sci.* 56:1547–60
Nadiga BT, Hecht MW, Margolin LG, Smolarkiewicz PK. 1997. On simulating flows with multiple time scales using a method of averages. *Theor. Comput. Fluid Dyn.* 9:281–92
Needler GT. 1967. A model for thermohaline circulation in an ocean of finite depth. *J. Mar. Res.* 25:329–42
Névir P. 2004. Ertel's vorticity theorems, the particle relabelling symmetry and the energy-vorticity theory of fluid mechanics. *Meteorol. Z.* 13:485–98
Névir P, Blender R. 1993. A Nambu representation of incompressible hydrodynamics using helicity and enstrophy. *J. Phys. A* 26:1189–93
Norbury J, Roulstone I, eds. 2002. *Large Scale Atmosphere-Ocean Dynamics I: Analytical Methods and Numerical Models*. Cambridge, UK: Cambridge Univ. Press
Oberlack M. 2006. *Symmetries, Invariance and Self-Similarity in Turbulence*. New York: Springer-Verlag
Ogura Y, Phillips NA. 1962. Scale analysis of deep moist convection and some related numerical calculations. *J. Atmos. Sci.* 19:173–79
Oliver M. 2006. Variational asymptotics for rotating shallow water near geostrophy: a transformational approach. *J. Fluid Mech.* 551:197–234
Pauluis O. 2008. Thermodynamic consistency of the anelastic approximation for a moist atmosphere. *J. Atmos. Sci.* 65:2719–29
Pedlosky J. 1984. The equations for geostrophic motion in the ocean. *J. Phys. Oceanogr.* 14:448–56
Pedlosky J. 1987. *Geophysical Fluid Dynamics*. New York: Springer. 2nd ed.
Peters N. 2000. *Turbulent Combustion*. Cambridge, UK: Cambridge Univ. Press
Petoukhov V, Ganopolski A, Brovkin V, Claussen M, Eliseev A, et al. 2000. Climber-2: a climate system model of intermediate complexity. Part I: model description and performance for the present climate. *Climate Dyn.* 16:1–17
Rahmstorf S, Archer D, Ebel DS, Eugster O, Jouzel J, et al. 2004. Cosmic rays, carbon dioxide and climate. *EOS Trans. AGU* 85:38–41
Roeckner E, Bäuml G, Bonaventura L, Brokopf R, Esch M, et al. 2003. The atmospheric general circulation model ECHAM5. Part I: model description. *Tech. Rep.*, Max Planck Inst. Meteorol., Hamburg, Germany
Salmon R. 1983. Practical use of Hamilton's principle. *J. Fluid Mech.* 132:431–44
Salmon R. 1998. *Lectures on Geophysical Fluid Dynamics*. Oxford, UK: Oxford Univ. Press
Schneider T. 2006. The general circulation of the atmosphere. *Annu. Rev. Earth Planet. Sci.* 34:655–88
Schochet S. 2005. The mathematical theory of low Mach number flows. *M2AN* 39:441–58
Shaevitz DA, Sobel AH. 2004. Implementing the weak temperature gradient approximation with full vertical structure. *Mon. Weather Rev.* 132:662–69
Shaw TA, Shepherd TG. 2009. A theoretical framework for energy and momentum consistency in subgrid-scale parameterization for climate models. *J. Atmos. Sci.* In press
Shepherd T. 1990. Symmetries, conservation laws, and Hamiltonian structure in geophysical fluid dynamics. *Adv. Geophys.* 32:287–338
Smolarkiewicz PK, Margolin LG. 1997. On forward-in-time differencing for fluids: an Eulerian/semi-Lagrangian non-hydrostatic model for stratified flows. *Atmos. Ocean* 35:127–57
Sobel A, Nilsson J, Polvani L. 2001. The weak temperature gradient approximation and balanced tropical moisture waves. *J. Atmos. Sci.* 58:3650–65
Sutherland BR. 2006. Weakly nonlinear internal gravity wavepackets. *J. Fluid Mech.* 569:249–58
Tessier Y, Lovejoy S, Schertzer D. 1993. Universal multi-fractals: theory and observations for rain and clouds. *J. Appl. Meteorol.* 32:223–50
Wang B, Xie X. 1996. Low-frequency equatorial waves in vertically sheared zonal flow. Part I: stable waves. *J. Atmos. Sci.* 53:449–67
Wedi N, Smolarkiewicz PK. 2009. A framework for testing global non-hydrostatic models. *Q. J. R. Metereol. Soc.* 135:469–84

Wheeler M, Kiladis GN. 1999. Convectively coupled equatorial waves analysis of clouds and temperature in the wavenumber-frequency domain. *J. Atmos. Sci.* 56:374–99

White AA. 2002. A view of the equations of meteorological dynamics and various approximations. See Norbury & Roulstone 2002, pp. 1–100

Zeitlin V, ed. 2007. *Nonlinear Dynamics of Rotating Shallow Water: Methods and Advances*. Amsterdam: Elsevier Sci.

Zeytounian RK. 1990. *Asymptotic Modeling of Atmospheric Flows*. New York: Springer

Annual Review of
Fluid Mechanics

Volume 42, 2010

Contents

Indexes

Errata

An online log of corrections to *Annual Review of Fluid Mechanics* articles may be found at http://fluid.annualreviews.org/errata.shtml